Chemical Science

EDGE ARTICLE

View Article Online
View Journal | View Issue

Check for updates

Cite this: *Chem. Sci.*, 2018, **9**, 5816

Spiropyran in nanoassemblies as a photosensitizer for photoswitchable ROS generation in living cells†

Jinkai Ji, Xiao Li, Tiantian Wu and Fude Feng *

Reversibly controlled generation of singlet oxygen from photosensitizing nanosystems has the benefits of selective cell killing and controllable effect time, but is a challenging option for photodynamic therapies. We report a strategy for integrating photochromic spiropyrans into biocompatible cationic polymers, which involved assembling nucleic acids into functional nanoparticles without introducing additional photosensitizers and imaging agents. We found that spiropyran-containing nanoparticles have photoswitching properties for both fluorescence (with a quantum yield of up to 0.27) and singlet oxygen generation (with a quantum yield of up to 0.22) in aqueous solutions and cells, and demonstrated that spiropyrans in nanoassemblies featuring aggregation-induced enhanced photosensitization and emission could be potentially applied in photodynamic therapy studies on tumor cells.

Received 12th March 2018
Accepted 11th June 2018

DOI: 10.1039/c8sc01148f

rsc.li/chemical-science

Open Access Article. Published on 11 juni 2018. Downloaded on 18.05.2026 02.30.41.
This article is licensed under a Creative Commons Attribution-NonCommercial 3.0 Unported Licence.

Introduction

Photodynamic therapy (PDT) is a kind of minimally invasive clinical treatment that employs photosensitizers (PSs), light, and oxygen to produce cytotoxic reactive oxygen species (ROS), especially $^1O_2$, and induce cell damage and tissue necrosis.[1–3] PDT has promising prospects in cancer therapy because of its high efficiency, selectivity, microtrauma, and negligible drug resistance.[4,5] In the past few decades, a large number of PSs, in the form of small molecules or nanostructures, have been designed as key components for PDT for singlet oxygen photosensitization.[6]

However, one of the major limitations of PDT is the undesired detrimental photosensitivity of PSs if they are distributed everywhere out of the target region or if the PSs remain photoactive after the PDT treatment. For example, approved PDT photosensitizers such as Photofrin and Temoporfin 1 have crucial defects due to their long clearance times (1–2 months).[7] It is also common that PS-modified nanomaterials maintain photoactivity over weeks.[8] Protection against exposure to natural light needs to be considered when PSs such as widely used porphyrins and phthalocyanines are applied.[6,9] To overcome the non-specificity and undesired long-lasting of photosensitization systems, improvement in the controllability of PS activation has become an attractive goal. An ideal solution will afford a remote "press button" that can repeatedly switch on and off the ROS generation by reversibly activating the PSs at any time, without drastically disrupting the physiological environment. Nano-delivery systems have been reported to control ROS generation *via* heat, ultrasound, and biochemical reactions, but by involving complicated components.[10–13] Recently, diarylethenes have been developed as useful photoswitches to tune the activities of target PSs in close proximity to diarylethenes,[14–17] but these face concerns with water solubility and stability, particularly when used in living biological systems.

In comparison to nonemissive diarylethenes, spiropyrans are photoswitchable between two isoforms that notably differ in fluorescence properties.[18] The fluorescent isoform of spiropyrans in solution has a short life span when excited, which impedes the investigation of the role of the triplet excited state that may interact with triplet oxygen. The emergence of fatigue in spiropyrans over the course of the repeated photoswitching process has been presumed to be attributable to the generation of harmful ROS.[19] This implies that an understanding of the activity of ROS is needed for the treatment of cells with spiropyran-containing photoactive materials. In the past few years, spiropyrans have been well studied as a crucial component in smart nanosystems (Table S1†) for drug delivery and cell imaging purposes, but there has been a lack of interest in their possible ROS generation and ROS-mediated consequences. To date, how to remotely control the level of ROS, intracellularly in particular, remains poorly understood.

Nanoassemblies with reversibly tunable optical properties have gained increasing attention.[20–22] Herein, we couple spiropyrans with cationic polymers to assemble plasmid DNA into functional nanoparticles (Fig. 1). Spiropyran nanoparticles are designed to satisfy the following requirements: (1) to tune ROS generation in solution or inside the cells in a reversible light-controlled manner without the need for extra PS species, (2) to switch within a short time into a deactivated state that does

Department of Polymer Science & Engineering, School of Chemistry & Chemical Engineering, Nanjing University, Nanjing, 210023, People's Republic of China. E-mail: fengfd@nju.edu.cn

† Electronic supplementary information (ESI) available. See DOI: 10.1039/c8sc01148f

This journal is © The Royal Society of Chemistry 2018

Open Access Article. Published on 11 juni 2018. Downloaded on 18.05.2026 02.30.41.
This article is licensed under a Creative Commons Attribution-NonCommercial 3.0 Unported Licence.

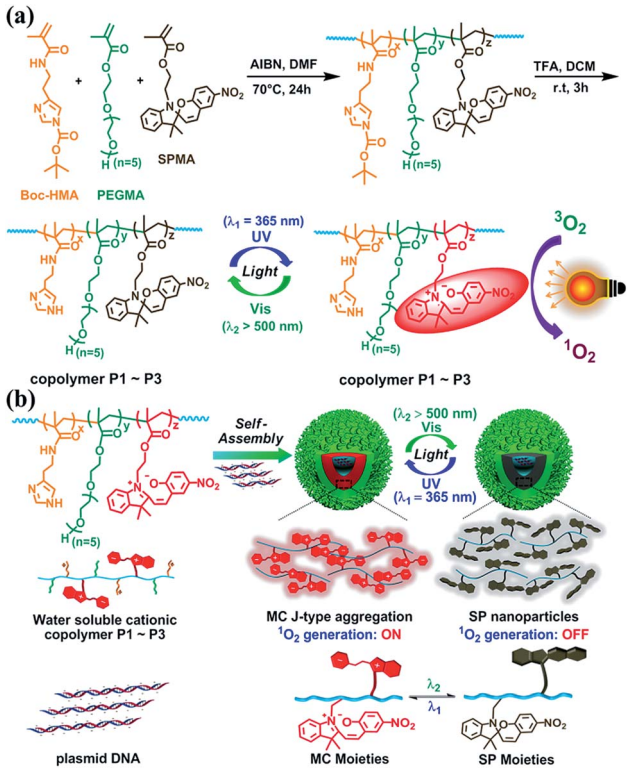

Fig. 1 Schematic presentations of (a) the synthetic route of **P1–P3**, the photoswitching of SP and MC, and light-induced ROS generation and (b) the self-assembly of spiropyran-containing polymers with DNA and reversibly light-controlled ROS generation. Boc-HMA, PEGMA and SPMA represent 2-(4-*tert*-butyloxycarbonyl imidazolyl)ethyl methacrylamide, poly(ethylene glycol) methacrylate, and 1′-(2-methacryloxyethyl)-3′,3′-dimethyl-6-nitro-spiro-(2*H*-1-benzopyran-2′,2′-indoline), respectively.

not respond to natural light, and (3) to allow for cell imaging and photo-induced cell killing.

Results and discussion

Synthesis of cationic polymers

As shown in Fig. 1a and S1–S3,† *via* AIBN-initiated free radical polymerization, linear copolymers were synthesized with pendent Boc-HMA, PEGMA, and SPMA moieties (detailed information for Boc-HMA, PEGMA, and SPMA is shown in Fig. 1). The ^{1}H NMR spectra of the monomers and the three purified polymer products indicated the successful integration of spiropyran, which accounts for 4.2, 11.7, and 21.6 mol% (Table S2†) of the products, separately. As estimated using GPC analysis (Fig. S4 and Table S2†), neutral polymers were obtained with unimodal distribution and similar molecular weights (M_n 11.7–13.1 kDa). Triflate acid treatment and purification *via* dialysis afforded cationic polymers **P1–P3** (Fig. 1a) accordingly, as evidenced by the disappearance of the characteristic proton resonance of the Boc groups in the ^{1}H NMR spectrum (Fig. S3†). We also prepared the control polymer **P4** by starting from the radical polymerization of Boc-HMA and PEGMA and using the same procedure (Table S2, Fig. S3 and S4†).

Each component of **P1–P3** has a special role. Hydrophilic oligo PEG and imidazole side chains ensure an adequate water solubility of the polymers. As the dominant component (48.8–58.3 mol%), oligo PEG helps shield the positive charges of the polyplexes to minimize nonspecific cytotoxicity and immunogenicity.[23] The high content of imidazole (29.6–37.5 mol%) in the polymers allows for DNA binding and condensing, and potentially boosts intracellular endolysosomal escape efficiency *via* the well-known proton sponge effect.[24] As for the spiropyran unit, it has been well described as a photochromic material that isomerizes between a hydrophobic ring closed form (SP isoform) and a zwitterionic ring opened form (merocyanine, MC isoform).[18] Generally, SP switches to MC after absorbing UV light, and this process is reversed *via* thermal relaxation in the dark or *via* excitation with visible light (>450 nm).

Characterization of the P1–P4 nanoassemblies

Atomic Force Microscopy (AFM) was employed to monitor the morphology changes of the polyplex assemblies prepared by complexing plasmid DNA with MC-dominating **P3** by changing the mass ratio (r) of **P3** to pDNA ranging from 1 to 30. As compared to the random coiled naked pDNA (Fig. 2a), plasmid forms a mesh-like structure (Fig. 2b) at r 1 due to the bridging of the DNA segments by the abundant imidazole groups in the polymer side chains.[25] As r increases from 1 to 5, node-like nuclei show up and grow in height from 3–8 nm (Fig. 2b) to 15–23 nm (Fig. S5†). The DNA coils disappear at r 15, and the increase of particle heights and sizes suggests the existence of aggregates. The increase in r from 15 to 30 results in a reduction in height from 40–70 nm to 30–45 nm and the formation of globular particles with an average diameter of approx. 126 nm (Fig. 2c–e). At r 30, the morphology of the **P3** NPs was consistent

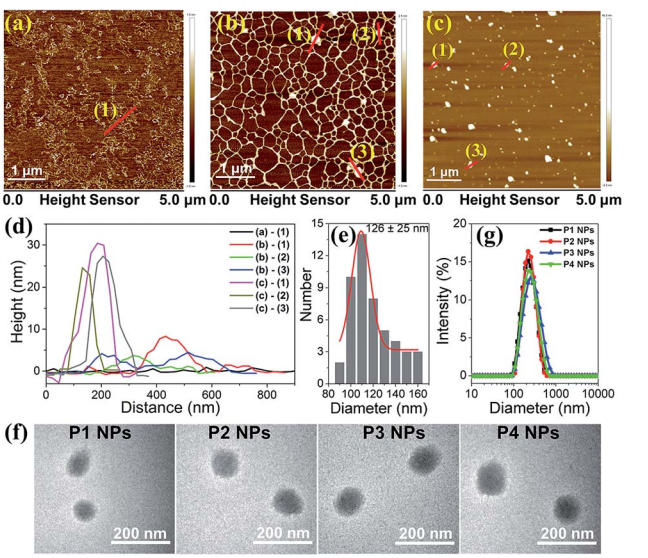

Fig. 2 AFM images of **P3** NPs formed at r 0 (a), 1 (b), and 30 (c). (d) The height cross-section along the lines shown with numbers in panels (a–c). (e) Size distribution of **P3** NPs (r = 30) shown in (c), determined using AFM. (f) TEM images of the **P1–P4** NPs (r = 30). (g) DLS analysis of the **P1–P4** NPs (r = 30).

Open Access Article. Published on 11 juni 2018. Downloaded on 18.05.2026 02.30.41.
This article is licensed under a Creative Commons Attribution-NonCommercial 3.0 Unported Licence.

with the observations from the transmission electron microscopy (TEM), which clearly showed similar results to the **P1–P4** NPs in which the **P1–P4** polymers had similar molecular weights (Fig. 2f). The DNA condensation behaviors are comparable to the extensively studied polylysine/DNA system due to the polycation character.[26]

At *r* 30, dynamic light scattering (DLS) analysis reveals the unimodal distribution of the **P1–P4** NPs and an average hydrodynamic diameter of approx. 200 nm (Fig. 2g), which is reasonably larger than the AFM and TEM results due to the difference in the solvation and dry states. We selected *r* 30 for all of our investigations on the nanoparticles unless stated otherwise. Due to the surface charge shielding effect of the oligo PEG chains,[27] the **P1–P4** NPs exhibit zeta potentials at 6–8 mV (Table S3†), which are less positive than for typical polyplexes and so favor the weakening of the nonspecific biomacromolecular interactions and the cytotoxicity.[28] It is worth noting that UV and visible light irradiation did not induce changes in the morphologies and hydrodynamic diameters of the **P1–P4** NPs, as evidenced from the TEM, AFM and DLS analyses (Fig. S6–8†). Alternative manipulation of the nanoassemblies (*r* 30) by assembling pure **P1–P4** polymers and **P1–P4** NPs with high amounts of DNA (at *r* 1 and *r* 5) leads to similar morphologies and sizes (Fig. S9 and S10†), which implies that efficient polymer binding to the intermediate assembly forms results in similar final nanostructures.

Photochromic properties of spiropyrans in P3 and the P3 NPs

We investigated the photochromic properties of the spiropyran moieties in the polymers, with **P3** as the example, by monitoring the changes in the UV-vis absorption spectra in HEPES buffer (10 mM, pH 7.0). The thermostable SP state of **P3** has minimal absorption at 549 nm, while the MC isoform of **P3** absorbs maximally with a 37 nm redshift relative to the small water soluble spiropyran molecule, SPQ (Fig. S1c and S11a†). The notable redshifts in the MC absorptions originate from the MC stacks in the polymers and nanoparticles. Brief LED UV light irradiation (λ_1 = 365 nm, 2 mW cm^{-2}, 2 min) led to rapid SP to MC isomerization, which could be identified *via* the appearance of a new absorption peak at 549 nm without visible shoulders or wavelength shifts (Fig. S11b†). In the reverse direction, MC to SP isomerization in **P3** was achieved *via* slow thermal relaxation in the dark or rapid photoisomerization under LED visible light exposure (λ_2 = 520 nm, 20 mW cm^{-2}) (Fig. S11c and d†).

The absorption spectroscopic and photochromic properties of spiropyrans were well preserved after **P3** was complexed with pDNA (Fig. S11a and 3a–b). The difference lies in the relaxation rates that were estimated using pseudo first order reaction kinetics. In the dark, the half life ($t_{1/2}$) of the MC state in the **P3** NPs was prolonged to 2.8 h as compared to 1.5 h in **P3** (Fig. 3c), presumably due to the slowed relaxation caused by steric factors.[29] In contrast, under visible light (λ_2 = 520 nm, 20 mW cm^{-2}), the $t_{1/2}$ of the MC state was sharply reduced to 3 min and 1.5 min for the **P3** NPs and **P3** (Fig. S12†), respectively.

It is of note that the MC-SP photoisomerization in the **P3** NPs could be complete within a few minutes under the exposure of

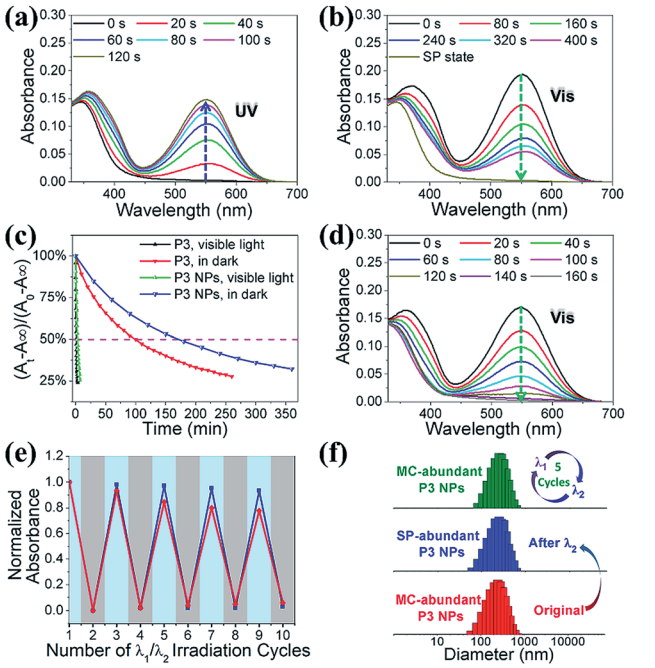

Fig. 3 Absorption spectra of the **P3** NPs under (a) UV light (λ_1 = 365 nm, 2 mW cm^{-2}, 0–120 s) irradiation and (b) visible light (λ_2 = 520 nm, 20 mW cm^{-2}, 0–400 s) irradiation. (c) MC-SP isomerization kinetics of **P3** and the **P3** NPs in the dark or under visible light. A_0, A_∞ and A_t are the absorption intensities at 549 nm, measured at the beginning, at the end and at the time of reaction, respectively. (d) Absorption spectra of the **P3** NPs under visible light (λ_2 > 500 nm, 250 mW cm^{-2}, 0–160 s) irradiation. (e) Photoswitching cycles of the **P3** NPs under irradiation by alternating 365 nm UV light and 520 nm visible light. Absorption intensities were monitored at 549 nm. The red and blue lines denote the measurements in the air-saturated and degassed solutions, respectively. (f) Comparison of hydrodynamic diameters of the **P3** NPs before and after different irradiation treatments.

an elevated irradiation power (λ_2 > 500 nm, 250 mW cm^{-2}) (Fig. 3d), which alleviates concerns about the possibility of the active MC state remaining after photoswitching treatment to ensure the insensitivity of the **P3** NPs toward natural light. In addition, in the dark, the full SP state showed undetectable absorption at 549 nm and the generation of the MC state over hours was nearly negligible in both **P3** and the **P3** NPs (Fig. S13a and b†), in contrast to the extreme sensitivity of the SP state to low power density UV light (λ_1 = 365 nm, 2 mW cm^{-2}) (Fig. S13c†). It should be mentioned that the heat generation upon alternating light irradiation was insignificant, as seen in the slight temperature fluctuation (<0.5 °C) (Fig. S14†). Thereby the concern of undesired photothermal effects that may cause alteration of nanoparticle structures, photoswitching kinetics and nonspecific cell damage is eliminated.

This efficient reversible photoisomerization allows for multiple cycles of photoswitching of the **P3** NPs under irradiation by alternating 365 nm UV light and 520 nm visible light. During 5 cycles of λ_1/λ_2 irradiation of the **P3** NPs and **P3**, the maximal MC absorption intensity remained unchanged in degassed HEPES buffer, and lost approx. 20% in air-saturated solution due to a slight fatigue effect (Fig. 3e). The stability of the **P3** NPs in photochromic processes was confirmed using

This journal is © The Royal Society of Chemistry 2018

Open Access Article. Published on 11 juni 2018. Downloaded on 18.05.2026 02.30.41.
This article is licensed under a Creative Commons Attribution-NonCommercial 3.0 Unported Licence.

DLS analysis, which revealed unaffected hydrodynamic diameters during the irradiation cycles (Fig. 3f).

Fluorescence and light-induced ROS generation of P1–P3 and the P1–P3 NPs

Generally, spiropyrans are not strong fluorophores, and their fluorescence originates from their MC states when they are excited by visible light. While the content of MC increases, the **P1–P3** polymers have a low fluorescence quantum yield (Φ_f) from 0.050 to 0.068, using rhodamine B as the standard (Φ_f = 0.89).[30] The Φ_f of SPQ is only 0.005, which is partly due to the short life span of MC in aqueous solution. In contrast, the **P1–P3** NPs display enhanced fluorescence (λ_{em} = 644 nm, Fig. S11a†) with Φ_f ranging from 0.18 to 0.27, which is 3.5–4.0 fold larger relative to the polymer counterparts (Fig. 4a) and means they outperform or are comparable to reported MC-containing film or particle systems (Table S1†).[31–33] This phenomenon is considered to be attributed to the aggregation-induced (enhanced) emission (AIE or AIEE) effect associated with J-type rather than H-type aggregation.[34,35]

The evidence supporting the fact that the J-aggregates are dominant comes from the following multiple observations: (1) the increase of Φ_f with increasing MC content in the polymers, (2) the redshift of the MC absorptions relative to the well dispersed SPQ, (3) the unimodal and constant MC absorption shape during isomerization, lacking the appearance of a shoulder peak at short wavelengths, (4) the bright fluorescence at long wavelengths, and (5) the well-fitted non-exponential kinetics of the MC/SP photoisomerization in the absorption at 549 nm.[19,31,36,37] It is not necessary to distinguish the dimers or multimers of the MC conformers that contribute to J-stacks in favor of irradiative relaxation.[38]

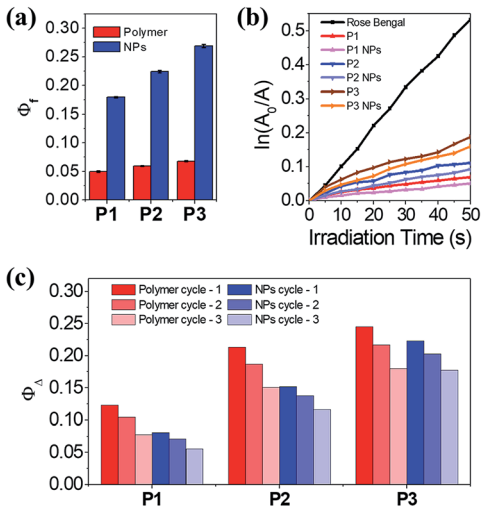

Fig. 4 (a) Φ_f of **P1–P3** and the **P1–P3** NPs in HEPES buffer (10 mM, pH 7.0) at 25 °C. (b) Plot of $\ln(A_0/A)$ as a function of time of visible light irradiation on the various photosensitizers, where A_0 and A are absorption intensity at 400 nm at the beginning and at irradiation time t, respectively. (c) Φ_Δ of **P1–P3** and the **P1–P3** NPs in HEPES buffer/D_2O (V/V = 1 : 9).

Interestingly, both the polymers and NPs exhibit a capability to generate $^1O_2$ upon activating the MC units under visible light. Using tetrasodium α,α′-(anthracene-9,10-diyl) bis(methylmalonate) (termed ABMM) as the $^1O_2$ trapping agent and Rose Bengal as the actinometer (0.75 in water),[39] the $^1O_2$ generation yields (Φ_Δ) of **P1–P3** in HEPES buffer (10 mM, pH 7.0)/D_2O (V/V = 1 : 9) were determined to be 0.12, 0.21, and 0.25, respectively (Fig. 4b–c). With the same trend between Φ_Δ and the MC content, the **P1–P3** NPs afforded Φ_Δ values of 0.08, 0.15, and 0.22, respectively, which are comparable to those of their polymer counterparts. In consideration of the big sizes of the NPs and the limited traffic distance of $^1O_2$,[40] the Φ_Δ values of the NPs are prone to be underestimated as a few amounts of $^1O_2$ are deactivated to the ground state before being accessible to the $^1O_2$ trapping agent. Nevertheless, after three cycles of λ_1/λ_2 irradiation on **P1–P3** and the **P1–P3** NPs, the NPs indicate improved fatigue performance (Fig. 4c). Evidently, the fluorescence and light-induced ROS generation behaviors are in parallel with each other because of J-stacks. This feature would facilitate the use of NPs, particularly **P3** NPs with the largest Φ_f and Φ_Δ values, in both cell imaging and light-controlled cell killing studies.

Cell imaging with the P3 NPs

The **P3** NPs have decent stability in both the HEPES buffer containing a high concentration of NaCl (0.2 M) and the complete DMEM medium containing 10% fetal bovine serum (FBS), as confirmed by the constant hydrodynamic diameters during five alternating λ_1/λ_2 irradiation cycles (Fig. S15a†). Similarly, as a control, the size of the **P4** NPs was not affected by the same treatment (Fig. S15b†). Such stability of nanoassemblies against salt and serum arises from the high content of PEG substituents and the low zeta potentials, affording excellent compatibility with cell culturing conditions.

By taking advantage of the MC fluorescence, we investigated cell uptake of the **P3** NPs under a confocal laser scanning microscope (CLSM). HeLa cells were pretreated with the **P3** NPs for 4 h before imaging. As shown in Fig. 5a, after brief UV light irradiation (λ_1 = 365 nm, 90 mW cm^{-2}, 1 min), the cells emitted bright red fluorescence from the MC state with excitation at 543 nm. The nuclei were not stained with red fluorescence, which is in good agreement with the frequently reported polymer-based nucleic acid delivery systems and is due to the endolysosome barrier for the internalized nanoparticles.[41,42] Subsequent LED visible light irradiation (λ_2 > 500 nm, 250 mW cm^{-2}, 10 min) led to an almost entire fluorescence quenching as a result of the efficient MC-SP photoswitching in the **P3** NPs. The fluorescence was found to be switched on and off again during the second and third cycles of λ_1/λ_2 alternating irradiation. The high level of MC fluorescence in the cells suggests that the nanoassembly structure could survive in intracellular internalization and photoswitching processes, according to the fluorescence of the MC state that has been shown to be highly dependent on the J-stacks. In contrast, the **P3** polymer alone when taken up by the HeLa cells gave a drastically attenuated signal (Fig. S16†), due to the low Φ_f of **P3** as well as the limited cell internalization.

Open Access Article. Published on 11 juni 2018. Downloaded on 18.05.2026 02.30.41.
This article is licensed under a Creative Commons Attribution-NonCommercial 3.0 Unported Licence.

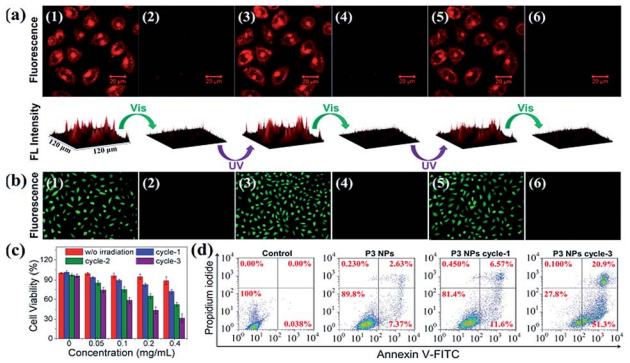

Fig. 5 Photoswitching cycles of the **P3** NPs taken up by the HeLa cells under alternating UV-light (365 nm, 90 mW cm^{-2}, 1 min) and visible light (>500 nm, 250 mW cm^{-2}, 10 min) treatments: (a) fluorescence images and intensity profiles (1,3,5-UV light; 2,4,6-visible light), and (b) oxidized DCF fluorescence images after visible light irradiation on the light-treated cells (1,3,5-MC state generated by UV light; 2,4,6-SP state generated by visible light). (c) MTT analysis and (d) flow cytometric analysis of the **P3** NP-treated HeLa cells with various photoswitching cycles under alternating UV light (365 nm, 90 mW cm^{-2}, 1 min) and visible light (>500 nm, 250 mW cm^{-2}, 3 min) treatments. The final concentrations of **P3** (in the form of NPs) are 0.2, 0.2 and 0.4 mg mL^{-1} applied in (a), (b) and (d), respectively.

Reversible ROS generation in cells controlled using the P3 NPs

To investigate the light-controlled reversible $^1O_2$ generation in cells, we detected intracellular ROS production in the **P3** NP-treated HeLa cells using commercial 2,7-dichlordihydrofluorescein diacetate (termed DCFH-DA) as a ROS probe. The green fluorescence intensity of the oxidized product DCF was proportional to the level of ROS generated.[43,44] After incubation with the **P3** NPs over a period of 4 h, the HeLa cells were subjected to LED UV light irradiation (365 nm, 90 mW cm^{-2}, 1 min) to accumulate the MC state. The MC-abundant cells were then subjected to photoswitching cycles before going into the ROS detection procedure, or directly went into the ROS detection procedure *via* incubation with DCFH-DA for 20 min in the dark, washing with PBS buffer, treatment with LED visible light (>500 nm, 250 mW cm^{-2}, 10 min) and imaging under an inverted fluorescence microscope. As shown in Fig. 5b, the bright green emission from DCF (λ_{ex} = 465–495 nm) throughout the cells was only observed with the MC-abundant cells, while the SP-abundant cells were detected with negligible fluorescence of DCF, correlating with the light-induced ROS generation capability of the MC state. As a control, DCF fluorescence was not detected in HeLa cells treated with PBS, PBS with visible light exposure, or MC-abundant **P3** NPs without visible light exposure (Fig. S17†). These results demonstrate that the intracellular ROS level could be reversibly controlled using light of selective wavelengths at desired times. The generation of a high intracellular ROS level is potentially useful for PDT purposes.

Accompanying the ROS generation under visible light, the **P3** NPs underwent simultaneous MC-SP isomerization and gradually lost their oxygen photosensitization capability unless they were re-activated. On the one hand, the thermally stable SP state is resistant to natural light and thereby avoids cell nonspecific phototoxicity. On the other hand, the re-activatable nature of the **P3** NPs allows for the inducing of cellular apoptosis *via* the repeated generation of ROS. To evaluate the cytotoxicity of the **P3** NPs, a conventional MTT assay was performed at 24 h after the light irradiation treatment of the HeLa cells. In the dark, the **P3** NPs exhibit marginal cytotoxicity in the polymer concentration range 0–0.4 mg mL^{-1} (Fig. 5c). However, treatment with successive 1–3 alternating irradiation cycles led to irradiation-cycle-dependent cytotoxicity, correlating with the level of accumulated ROS generated (Fig. 5c). Each cycle included sequential UV light (λ_1 = 365 nm, 90 mW cm^{-2}, 1 min) and visible light (λ_2 > 500 nm, 250 mW cm^{-2}, 3 min) treatments. To minimize the possibility of concurrent activation of the MC isoform in the SP-MC conversion process, the UV light irradiation duration time was short. Consequently, only approx. 30% of the HeLa cells survived three irradiation cycles. This result was in good agreement with the flow cytometric analysis, which detected 72.2% apoptotic cells under the same protocols (Fig. 5d). Obviously, it is convenient to alter the cytotoxic effect by controlling the number of irradiation cycles. As a control, using the same procedure except that the **P3** NPs were absent or the **P3** NPs were replaced by **P4** NPs, cell viabilities were greater than 95% (Fig. 5d and S18†), suggesting that the tumor cells were insensitive to light treatments without spiropyrans, but vulnerable to ROS generation using oxygen photosensitization.

Conclusions

In summary, spiropyran-decorated cationic copolymers were synthesized and complexed with plasmid DNA to form nanoassemblies *via* electrostatic interaction. The nanoparticles were stable in buffer solutions containing salt or serum, and showed good biocompatibility. By virtue of the photochromic properties of the spiropyran units, the nanoparticles conferred the following merits of the spiropyran chromophore: (1) a suitable MC half life of up to 2.8 h in the dark; (2) a relatively high Φ_f of up to 0.27; (3) an applicable Φ_Δ of up to 0.22; (4) reversibility in controlling the fluorescence and ROS generation using light; (5) a dual functionality in cell imaging and apoptosis. To the best of our knowledge, this is the first example that utilizes spiropyran as a photosensitizer and provides a proof-of-concept approach to reversibly controllable aggregation-induced enhanced photosensitization and emission (AIEPE). This simple concept provides a useful option for biomedical applications such as light-controlled PDT and drug delivery. The two-photon photoswitching properties of the spiropyran-containing nanosystems[45] will be an additional bonus for expanding the use of AIEPE in *in vivo* studies using near infrared light for tissue penetration to activate the J-stacks of the MC isoform.

Conflicts of interest

There are no conflicts to declare.

Acknowledgements

We thank the National Basic Research Program of China (2015CB856300), the National Natural Science Foundation of

This journal is © The Royal Society of Chemistry 2018

Open Access Article. Published on 11 juni 2018. Downloaded on 18.05.2026 02.30.41.
This article is licensed under a Creative Commons Attribution-NonCommercial 3.0 Unported Licence.

China (21474046), the 1000 Young Talent Program, the Collaborative Innovation Center of Chemistry for Life Sciences, and the Program for Changjiang Scholars and Innovative Research Team in University for financial support.

Notes and references

1 P. R. Ogilby, *Chem. Soc. Rev.*, 2010, **39**, 3181.
2 H. Chen, J. Tian, W. He and Z. Guo, *J. Am. Chem. Soc.*, 2015, **137**, 1539.
3 M. Lismont, L. Dreesen and S. Wuttke, *Adv. Funct. Mater.*, 2017, **27**, 1606314.
4 A. Castano, P. Mroz and M. Hamblin, *Nat. Rev. Cancer*, 2006, **6**, 535.
5 H. Fan, G. Yan, Z. Zhao, X. Hu, W. Zhang, H. Liu, X. Fu, T. Fu, X. Zhang and W. Tan, *Angew. Chem., Int. Ed.*, 2016, **55**, 5477.
6 M. Ethirajan, Y. Chen, P. Joshi and R. Pandey, *Chem. Soc. Rev.*, 2011, **40**, 340.
7 T. Kocki, B. Czarczynska-Goslinska, K. Kocka, M. Stolarska, D. Wachowska, S. Lijewski, T. Koczorowski and T. Goslinski, in *Nurses and pharmacists in interdisciplinary team of health care providers in photodynamic therapy*, ed. Y. Tanaka, Photomedicine Intech., 2017.
8 D. Min, D. Jeong, M. G. Choi and K. Na, *Biomaterials*, 2015, **52**, 484.
9 X. Ding and B. H. Han, *Angew. Chem., Int. Ed.*, 2015, **54**, 6536.
10 Z. Zhou, J. Song, L. Nie and X. Chen, *Chem. Soc. Rev.*, 2016, **45**, 6597.
11 S. Kolemen, T. Ozdemir, D. Lee, G. Kim, T. Karatas, J. Yoon and E. Akkaya, *Angew. Chem., Int. Ed.*, 2016, **55**, 3606.
12 W. Li, C. Su, Y. Chang, Y. Lin and C. Yeh, *ACS Nano*, 2016, **10**, 2017.
13 J. Ge, M. Lan, B. Zhou, W. Liu, L. Guo, H. Wang, Q. Jia, G. Niu, X. Huang and H. Zhou, *Nat. Commun.*, 2014, **5**, 4596.
14 J. Park, Q. Jiang, D. Feng and H. Zhou, *Angew. Chem., Int. Ed.*, 2016, **128**, 7304.
15 J. Park, D. Feng, S. Yuan and H. Zhou, *Angew. Chem., Int. Ed.*, 2015, **54**, 430.
16 L. Hou, X. Zhang, T. C. Pijper, W. R. Browne and B. L. Feringa, *J. Am. Chem. Soc.*, 2014, **136**, 910.
17 J. Qi, C. Chen, X. Y. Zhang, X. L. Hu, S. L. Ji, R. T. K. Kwok, J. W. Y. Lam, D. Ding and B. Z. Tang, *Nat. Commun.*, 2018, **9**, 1848.
18 R. Klajn, *Chem. Soc. Rev.*, 2014, **43**, 148.
19 V. I. Minkin, *Chem. Rev.*, 2004, **104**, 2751.
20 G. Wu, S. C. Chen, C. L. Liu and Y. Z. Wang, *ACS Nano*, 2015, **9**, 4649.
21 C. H. Li, Y. X. Zhang, J. M. Hu, J. J. Cheng and S. Y. Liu, *Angew. Chem., Int. Ed.*, 2010, **49**, 5120.
22 X. R. Wang, J. M. Hu, G. H. Liu, J. Tian, H. J. Wang, M. Gong and S. Y. Liu, *J. Am. Chem. Soc.*, 2015, **137**, 15262.
23 J. S. Suk, Q. G. Xu, N. Kim, J. Hanes and L. M. Ensign, *Adv. Drug Delivery Rev.*, 2016, **99**, 28.
24 I. K. Park, K. Singha, R. B. Arote, Y. J. Choi, W. J. Kim and C. S. Cho, *Macromol. Rapid Commun.*, 2010, **31**, 1122.
25 A. Muramatsu, Y. Shimizu, Y. Yoshikawa, W. Fukuda, N. Umezawa, Y. Horai, T. Higuchi, S. Fujiwara, T. Imanaka and K. Yoshikawa, *J. Chem. Phys.*, 2016, **145**, 235103.
26 I. Nayvelt, T. Thomas and T. J. Thomas, *Biomacromolecules*, 2007, **8**, 477.
27 J. S. Choi, D. K. Joo, C. H. Kim, K. Kim and J. S. Park, *J. Am. Chem. Soc.*, 2000, **122**, 474.
28 S. Venkataraman, W. L. Ong, Z. Y. Ong, S. C. J. Loo, P. L. R. Ee and Y. Yang, *Biomaterials*, 2011, **32**, 2369.
29 H. R. Allcock and C. Kim, *Macromolecules*, 1991, **24**, 2846.
30 D. D. Cheng, X. L. Liu, Y. D. Xie, H. T. Lv, Z. Q. Wang, H. Z. Yang, A. X. Han, X. M. Yang and L. Zang, *Sensors*, 2017, **17**, 2517.
31 L. Y. Zhu, W. W. Wu, M. Q. Zhu, J. J. Han, J. K. Hurst and A. D. Q. Li, *J. Am. Chem. Soc.*, 2007, **129**, 3524.
32 J. L. Bahr, G. Kodis, L. de la Garza, S. Lin, A. L. Moore, T. A. Moore and D. Gust, *J. Am. Chem. Soc.*, 2001, **123**, 7124.
33 T. Minami, N. Tamai, T. Yamazaki and I. Yamazaki, *J. Phys. Chem.*, 1991, **95**, 3988.
34 C. H. Li and S. Y. Liu, *Chem. Commun.*, 2012, **48**, 3262.
35 Y. N. Hong, J. W. Y. Lam and B. Z. Tang, *Chem. Soc. Rev.*, 2011, **40**, 5361.
36 M. Q. Zhu, L. Zhu, J. J. Han, W. W. Wu, J. K. Hurst and A. D. Q. Li, *J. Am. Chem. Soc.*, 2006, **128**, 4303.
37 L. V. Natarajan, T. J. Bunning and S. Y. Kim, *Macromolecules*, 1994, **27**, 7248.
38 P. Uznanski, *Synth. Met.*, 2000, **109**, 281.
39 M. Wang, S. Maragani, L. Y. Huang, S. Jeon, T. Canteenwala, M. R. Hamblin and L. Y. Chiang, *Eur. J. Med. Chem.*, 2013, **63**, 170.
40 L. Xia, X. G. Kong, X. M. Liu, L. P. Tu, Y. L. Zhang, Y. L. Chang, K. Liu, D. Z. Shen, H. Y. Zhao and H. Zhang, *Biomaterials*, 2014, **35**, 4146.
41 N. Nishiyama, A. Iriyama, W. Jang, K. Miyata, K. Taka, Y. Inoue, H. Takahashi, Y. Yanag, Y. Tamaki, H. Koyama and K. Kataoka, *Nat. Mater.*, 2005, **4**, 934.
42 M. Karimi, A. Ghasemi, P. S. Zangabad, R. Rahighi, S. M. M. Basri, H. Mirshekari, M. Amiri, Z. S. Pishabad, A. Aslani, M. Bozorgomid, D. Ghosh, A. Beyzavi, A. Vaseghi, A. R. Aref, L. Haghani, S. Bahramia and M. R. Hamblin, *Chem. Soc. Rev.*, 2016, **45**, 1457.
43 W. O. Carter, P. K. Narayanan and J. P. Robinson, *J. Leukocyte Biol.*, 1994, **55**, 25.
44 *Singlet Oxygen. Applications in Biosciences and Nanosciences*, ed. S. Nonell and C. Flors, London, 2016.
45 G. Marriott, S. Mao, T. Sakata, J. Ran, D. K. Jackson, C. Petchprayoon, T. J. Gomez, E. Warp, O. Tulyathan, H. L. Aaron, E. Y. Isacoff and Y. Yan, *Proc. Natl. Acad. Sci. U. S. A.*, 2008, **105**, 17789.